ADVANCED OPTICAL MATERIALS
www.advopticalmat.de

Optical Reflectance of Composites with Aligned Engineered Microplatelets

Erik Poloni, Henning Galinski, Florian Bouville,* Bodo Wilts, Leonid Braginsky, David Bless, Valery Shklover, Alba Sicher, and André R. Studart**

The reflection of light from distributed microplatelets is an effective approach to creating color and controlling the optical properties in paints, security features, and optical filters. However, predictive tools for the design and manufacturing of such composite materials are limited due to the complex light–matter interactions that determine their optical response. Here, the optical reflectance of individual reflective microplatelets and of polymer-based composites containing these engineered platelets as an aligned, dispersed phase are experimentally studied and analytically calculated. Transfer-matrix calculations are used to interpret the effect of the platelet architecture, the number of platelets, and their size distribution on the experimentally measured reflectance of composites prepared using a previously established magnetic alignment technique. It is demonstrated that the reflectance of the composites can be understood as the averaged response of an array of Fabry–Pérot resonators, in which the microplatelets act as semi-transparent flat reflectors and the polymer as cavity medium. By using an analytical model and computer simulations to describe the interaction of light with platelets embedded in a polymer matrix, this work provides useful tools for the design and fabrication of composites with tailored optical reflectance.

1. Introduction

Reflective platelets are largely used in industry for the control of color and sparkle effects with applications in car and wall paints, cosmetics, security, and optical filters.[1,2] Reflective structures have also been applied for the radiative cooling of buildings,[3,4] the design of camouflaging effects,[5,6] and the thermal protection of engines.[7,8] To enhance reflectance and create specific color effects, reflective particles are engineered to feature dimensions on the order of the wavelength of visible light. These particles are often coated with materials with a contrasting refractive index, which further increases the reflectance.[9] In such coated platelets, structural color arises from the interference of light reflected from the interfaces within an individual platelet.

Besides technological applications, structural colors are used by living

E. Poloni, F. Bouville, D. Bless, A. R. Studart
Complex Materials
Department of Materials
ETH Zürich
Zürich 8093, Switzerland
E-mail: andre.studart@mat.ethz.ch

H. Galinski
Laboratory for Nanometallurgy
Department of Materials
ETH Zürich
Zürich 8093, Switzerland
E-mail: henning.galinski@mat.ethz.ch

B. Wilts
Adolphe Merkle Institute
University of Fribourg
Fribourg 1700, Switzerland

The ORCID identification number(s) for the author(s) of this article can be found under https://doi.org/10.1002/adom.202201989.

DOI: 10.1002/adom.202201989

L. Braginsky, V. Shklover
Institute of Electromagnetic Fields
ETH Zürich
Zurich 8092, Switzerland

L. Braginsky
Institute of Semiconductor Physics
Novosibirsk State University
Novosibirsk 630090, Russia

A. Sicher
Laboratory for Soft and Living Materials
Department of Materials
ETH Zürich
Zürich 8093, Switzerland

E. Poloni
High Enthalpy Flow Diagnostics Group
Institute of Space Systems
University of Stuttgart
70569 Stuttgart, Germany

E. Poloni, F. Bouville
Centre for Advanced Structural Ceramics
Department of Materials
Imperial College London
London SW7 2BX, UK
E-mail: f.bouville@imperial.ac.uk

B. Wilts
Department Chemistry and Physics of Materials
University of Salzburg
Salzburg 5020, Austria

organisms in the natural world to fulfill specific biological functions.[10–12] Fascinating examples of relevance for this work are the neon tetra fish,[13] the blue-ringed octopus,[14] and the color-changing zebrafish,[15,16] which utilize stacks of platelets inside iridophores to dynamically control iridescence. This mechanism has inspired the development of color-changing synthetic materials for dynamic camouflaging and tunable optical displays.[6,17] In both synthetic and biological materials, control over the orientation of engineered platelets is essential to tune the reflectance and structural color of the optical system.[10,11]

Attempts to correlate the optical properties of platelet-containing composite materials with their underlying microstructure have been made using established radiative transfer models,[7,18,19] including the well-known transfer-matrix approach.[20,21] The transfer matrix method[22] is a versatile analytical tool to study the propagation of quantum particles, such as electrons or photons, in arbitrary one-dimensional potentials or periodic media including metamaterials,[23] photonic crystals[24] and superlattices.[25] Current models for platelet-containing composites show that, despite their overall disordered arrangement, platelets with thickness on the order of the incident wavelength cause optical interference effects that substantially enhance or reduce the optical reflectance of the composite, particularly at high filler concentrations. Previous work has also shown that only a fraction of metallic disc-shaped particles contribute to the reflectance of composites, which allows a minimization of the thickness of composite coatings without compromising their optical properties.[18] Despite these important contributions, the current design and understanding of the optical reflectance of structural colored particle-containing composites disregard the influence of particle angular distributions and potential multiple scattering events that occur in multilayered platelets. Further research is therefore needed to develop knowledge for the manufacturing of composites that contain platelets with engineered surface coatings.

In this study, we experimentally characterize and model the optical reflectance of composites with oriented, engineered microplatelets, considering the platelet architecture and misalignment caused by the manufacturing process. First, we describe a magnetic approach that can be used to manufacture composites with highly aligned engineered platelets in a polymer matrix. The optical properties of individual engineered platelets are then experimentally measured and compared to transfer-matrix calculations based on idealized, model platelet architectures. Particular attention is given to the effect of a reflective titania coating on the reflectance of alumina platelets. Next, the reflectance of composites containing bare and titania-coated microplatelets in epoxy is measured and compared against analytical calculations. Finally, we quantify the level of orientation of platelets in these epoxy-based composites and predict the number of platelets expected to contribute to the composite's reflectance.

2. Results and Discussion

2.1. Engineered Platelets and Composite Fabrication

The investigated composites consist of disc-shaped specimens that contain engineered alumina-based platelets distributed within a continuous epoxy phase (**Figure 1**). The platelets are predominantly aligned with their face parallel to the disc surface and the alignment angle of each platelet is given by θ_i. While the alignment angle is on average close to zero, an angular distribution is expected from the manufacturing process utilized for the fabrication of the composites (Figure 1b,c).

Composites with distributed microplatelets were manufactured using a magnetic alignment approach as previously reported in the literature (**Figure 2**c).[26–28] In this method, magnetically responsive anisotropic particles are suspended in a liquid medium and oriented in a specific direction with the help of an external magnet before solidification of the liquid phase. Commercially available alumina platelets and epoxy resin were used as anisotropic particles and curable liquid medium, respectively. Because alumina is diamagnetic, the platelets were made magnetically responsive by covering their surface with superparamagnetic iron oxide nanoparticles (SPIONs, see Materials and methods).[26]

Biaxial alignment of the coated platelets is achieved by applying a rotating magnetic field of the order of 15 mT while the liquid is cured. Three types of commercial alumina platelets with different dimensions were investigated in this study (**Table** 1, Figure 2a,b). Two platelet types here called LT and LTT, are coated with a layer of rutile titania of thickness (δ) in the range

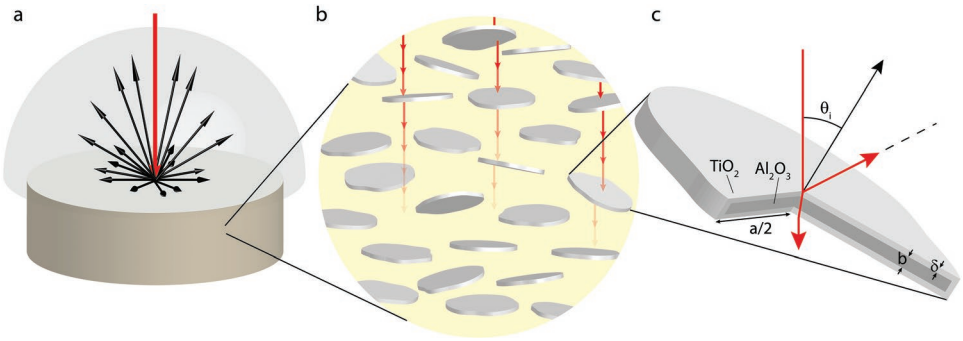

Figure 1. Schematics of composites with distributed microplatelets. a) Disc-shaped geometry of the macroscopic specimen, indicating the multiple reflections (black arrows) of the incident light (red arrow). b) Microplatelets embedded in a continuous polymer phase. The red arrows represent light rays that are attenuated through scattering and absorption phenomena within the material. c) Individual alumina platelet coated with a thin titania layer. The orientation of the platelet is quantified in terms of the angle θ_i relative to the normal of specimen surface.

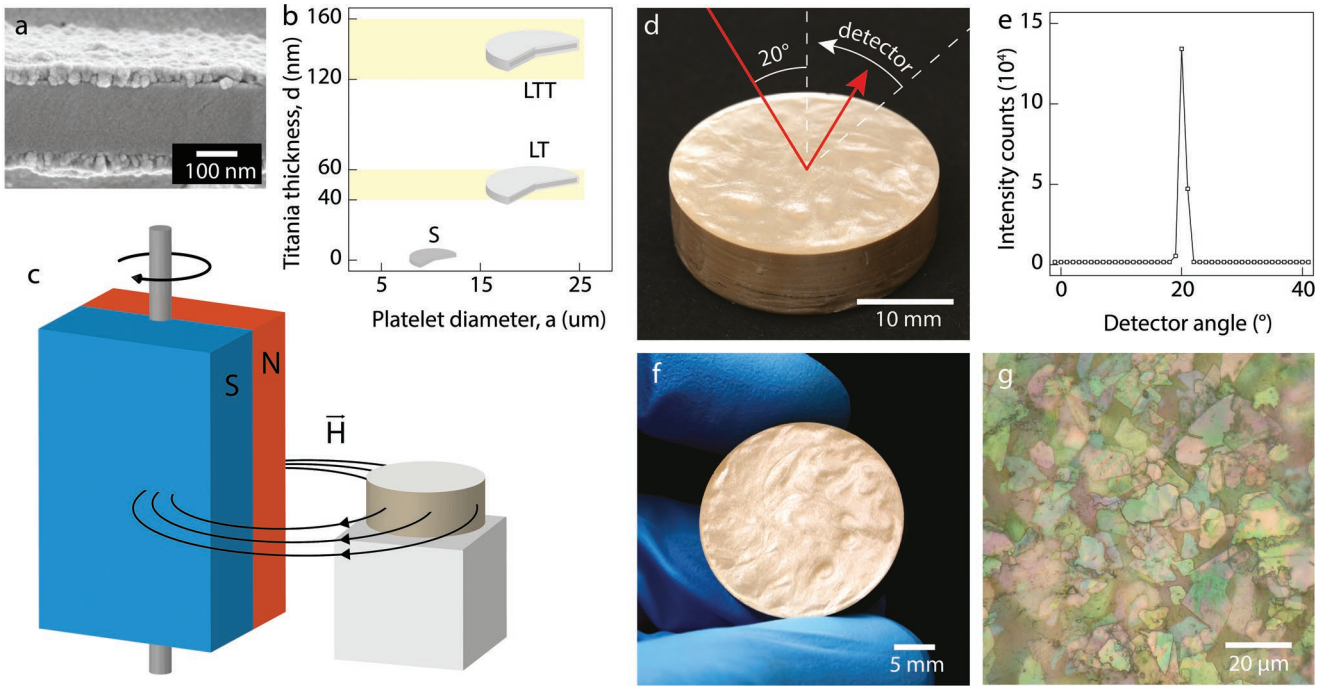

Figure 2. Manufacturing and reflectance of platelet-containing composites. a) Micrograph of an alumina platelet coated with titania. Adapted with permission from Pfaff.[29] Copyright 2013, succidia AG. b) Diagram displaying the approximate dimensions of the three platelet types investigated in the study. The nomenclature used to describe the platelets indicates whether they are small (S) or large (L), and the possible presence of a thin (T) or thick (TT) titania layer. c) Magnetic setup utilized for platelet alignment in the composite. d) Procedure used to measure the angle-dependent reflectance of composites, in which the incident light was kept at 20° from the normal and the detector angle was varied. e) Angle-dependent reflectance of a sample containing 5 vol% LT platelets distributed in epoxy. f) Photograph and g) optical microscopy image of the top surface of the composite sample characterized in (d,e).

40–60 nm and 120–160 nm, respectively. Since rutile has a high refractive index, the titania coating enhances the iridescence effect resulting from interference of light within the wavelength range of interest. Indeed, disc-shaped composite samples containing titania-coated platelets aligned parallel to the surface exhibit structural color and distinguishable reflective patterns under normal illumination (Figure 2f,g). Optical microscopy of such samples confirms the presence of a high concentration of relatively well-aligned platelets close to the surface of the composite. We hypothesize that the high reflectance of the composite arises from the reflection of light by the aligned platelets, which serve as flat micro-reflectors for the incoming light.

To assess whether individual platelets can be approximated by micron-sized flat reflectors, the angle-dependent reflectance of composite samples was characterized (Figure 2d). In this experiment, the angle of incident light was kept at −20° relative to the sample normal, while the angle of the detector was varied between 0–40°. A strong reflection peak was observed when the detector was placed at 20°, which corresponds to specular light reflection (Figure 2e). While the polished surface of the sample might contribute to this reflection, the inhomogeneous visual appearance of the polished sample (Figure 2f) suggests that the reflection by individual platelets plays a dominant role in the measured reflectivity. The directional reflectance observed in this experiment indicates that the collective optical response of the well-aligned platelets can be approximated by assuming that they behave as flat micron-sized reflectors.

Table 1. Bare and titania-coated alumina platelets investigated in this work.

Platelet type	Diameter, *a* [µm]	Thickness, *b* [nm]	Thickness of TiO_2 coating, δ [nm]
S	5–15	300–450	0
LT	15–25	200–400	40–60
LTT	15–25	200–400	120–160

2.2. Experimental Analysis and Modeling of Individual Platelets

To quantify the physical mechanism leading to the high reflectance of the composite, we first experimentally measured the reflectance of individual platelets and compared it with analytical calculations performed on a model system. Experiments were carried out by coupling a spectrometer to a microscope and adjusting the illuminated spot size to target single platelets (see Materials and methods).

The experimental reflectance spectra of individual platelets show multiple peaks within the range of visible wavelengths (**Figure 3**a,b; Figure S1a, Supporting Information). This reflects the fact that these commercial platelets are deliberately engineered to produce structural colors. The presence of a relatively thin titania coating on the alumina platelets not only blue-shifts the spectral peaks but also increases significantly the maximum reflectance of individual platelets from ≈ 15% to

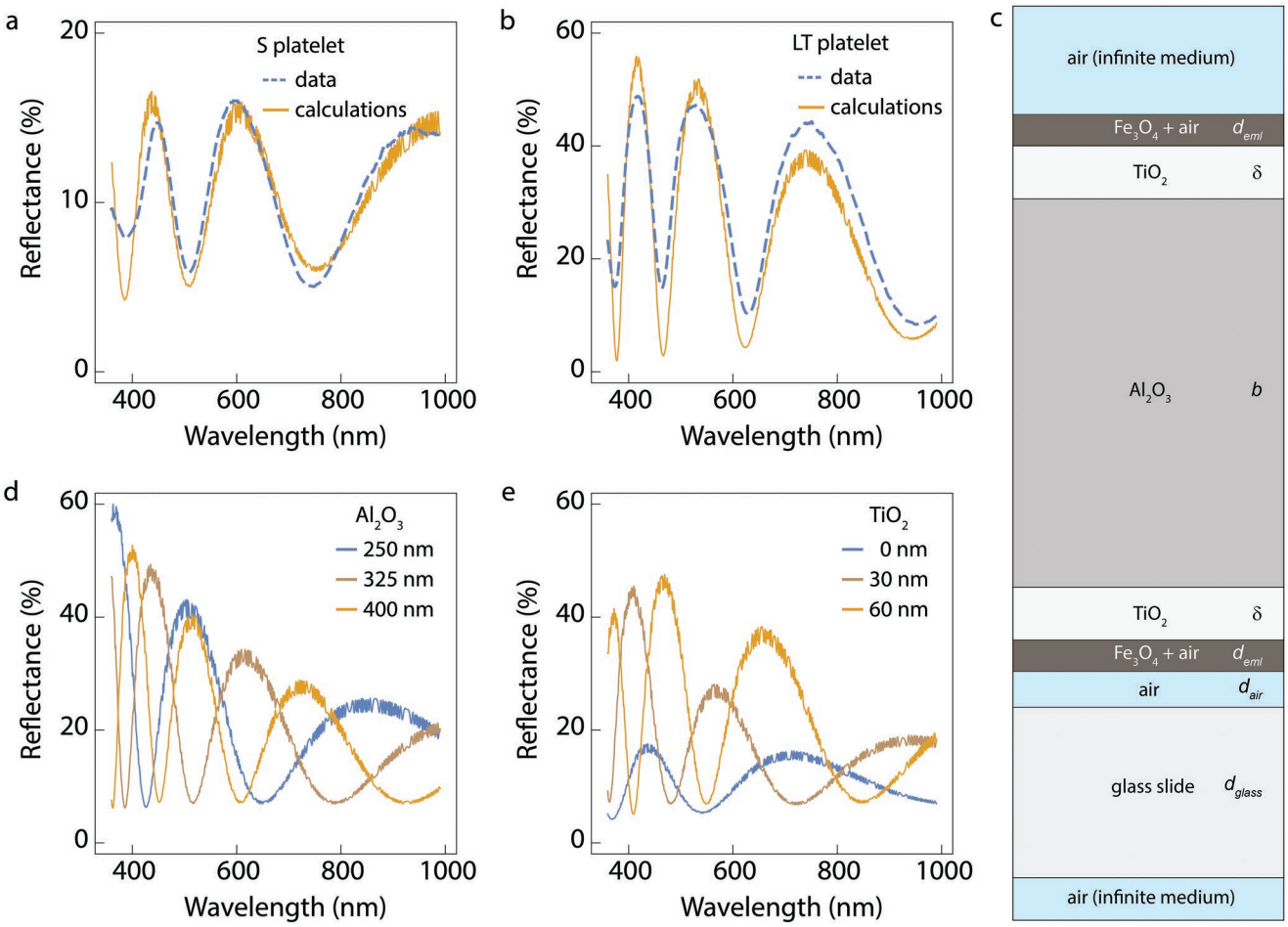

Figure 3. Reflectance of single microplatelets. Comparison of experimental data and calculated reflectance curves of a) an S platelet and b) an LT platelet. c) Schematics of the platelet structure used in the transfer-matrix calculations. The alumina platelet is coated with a reflective titania layer and an effective medium layer formed by iron oxide and air. Calculated data obtained by varying the thickness of the d) alumina layer, b, and of the e) titania layer, δ, of an LT platelet.

50% (Figure 3a,b). This is caused by the refractive index contrast between titania and alumina. Notably, the line shape of the reflectance spectra, with reoccurring minima and maxima, resembles the characteristics of a Fabry–Pérot resonator.[30]

A comparison of our experimental data with the analytical reflectance spectra of single platelets allows us to calibrate the proposed optical model. In a later step, this model can be used to evaluate the effect of individual material and geometrical parameters on the reflectance spectra of composites containing these engineered platelets. With this in mind, we modeled the optical response of the individual platelets using the well-established transfer-matrix method.[20] This analytical approach yielded exact solutions for the reflectance of multilayered platelets and gave us physical insights that are not captured by numerical approaches.

For the transfer-matrix calculations, the geometry of the platelets can be locally simplified to a one-dimensional structure with an alumina core of thickness b with perfectly flat interfaces and infinite lateral limits (Figure 3c). Considering that the single platelet is placed on top of a glass slide, a relatively thin air layer will form between the platelet and the glass surface. Moreover, the SPIONs placed onto single platelets are included in this one-dimensional approach by forming an effective medium layer on top of the titania coating. While SPIONs are known to form agglomerates of a few tenths of nanometers thickness onto the platelet surface, the volume they define around a platelet can be approximated by a homogeneous single layer formed by a mixture of iron oxide and air (Figure 3c).[26] The refractive index of this mixture is then estimated by applying a Maxwell Garnett effective medium approach.[31]

The above-described model allows us to calculate the reflectance of a single idealized platelet in air. In these calculations, the reflectance of the model platelet can be tuned to the experimental data (Figure 3a,b; Figure S1a, Supporting Information) by altering the thickness of the alumina, titania, and air layers as fitting parameters. The wavelength-dependent refractive indices of alumina, titania, and iron oxide used in these calculations were taken from previous works.[32,33] For air and glass, $n = 1$ and $n = 1.5$, respectively. The refractive index of the effective medium layer formed by iron oxide and air was calculated assuming a SPION surface coverage of 13%.[26] The thickness

Table 2. Thickness of individual layers of the model platelet obtained by fitting the calculations to the experimental data.

Platelet	Alumina, b [nm]	Titania, δ [nm]	Iron oxide + air, d_{eml} [nm]	Air, d_{air} [nm]
S	450	0	12	10
LT	390	60	12	40
LTT	280	150	12	90

of the effective medium layer was considered to be 12 nm, the diameter of a single SPION.[34]

The calculated reflectance spectra agree reasonably well with the experimental data for both bare alumina and titania-coated alumina platelets (Figure 3a,b; Figure S1a, Supporting Information). Importantly, this agreement was achieved using physically meaningful values for the thicknesses of the alumina platelets, titania coating, and air gap (**Table 2**). These results provide useful insight, as they suggest that a single platelet can be treated as a lossy Fabry–Pérot (FP) resonator, whereby either the surrounding SPION layer or the titania coating act as a set of thin flat reflectors and the alumina layer acts as cavity medium. The optical losses in the platelet arise primarily from round-trip loss in the cavity medium (see Figure S2, Supporting Information). This can be quantified by the finesse F, which represents the number of round trips light takes until it is either leaked out or absorbed. The addition of titania to the platelet significantly enhances the reflectivity of the flat reflectors due to the higher index contrast and thus enhances the finesse of the FP, which is $F = 2.0$ in case of an S platelet and $F = 4.2$ in case of an LT platelet (Figure 3a,b).

Given the satisfactory agreement between experiment and model, we performed additional calculations to investigate the influence of the thicknesses of the alumina, the titania, and the SPION layers on the reflectance spectra of an individual LT platelet (Figure 3d,e; Figure S1b, Supporting Information). The calculations showed that both the thickness of the alumina platelet and the thickness of the titania coating affect the magnitude and the positions of the FP resonances in the reflectance spectra, whereas the SPION layer thickness only slightly changes the peak height. This effect is to be expected as the distance between single resonances $\Delta\lambda$ in a FP resonator, also called free spectral range (FSR), is given by $\Delta\lambda = \lambda_m - \lambda_{m-1} = \frac{\lambda_m^2}{nd}$, where n and d are the refractive index and the length of the cavity, respectively.

The calculations also reveal that coating the alumina platelet with a 30 nm thick titania layer is sufficient to increase the reflectivity of the flat micro-reflectors and the maximum reflectance by a factor of two (Figure 3e). These results provide useful insights for the selection and design of platelets to be used as optical elements in highly reflective composites.

2.3. Optical Properties of Composites

The optical properties of composites containing engineered microplatelets aligned in an epoxy matrix were experimentally assessed by measuring the total reflectance in the visible and near infrared (NIR) region of specimens with different types and different concentrations of platelets (**Figure 4**).

Similar to the results obtained for individual platelets (Figure 3), the experiments reveal a strong effect of the alumina platelets and, in particular, of the titania coating on the optical reflectance of the composite (Figure 4a–c). Specimens with bare alumina platelets show reflectance values up to 6-fold higher than that of pure epoxy, indicating that the refractive index contrast between alumina and epoxy is already sufficient to enable strong reflection. Additionally, the presence of the titania coating on the alumina platelets increases the maximum reflectance of the composite further from ≈30% to 70%. Overall, a strong, broad-band reflectance across the whole visible and NIR spectrum was observed for all the investigated specimens. Because the measurements were conducted using an integrating sphere, the spectra correspond to the sum of the specular reflectance and the scattered light, which smooths out their FP mode.

To evaluate the effect of the volume fraction of platelets on the optical properties of the composite, we averaged the measured total reflectance over the wavelength ranges 450–900 nm and 1000–1630 nm (Figure 4d–f). The obtained results indicate that the average reflectance increases sharply with the platelet concentration and eventually levels off at volume fractions above 5 vol%. Generally, 1 vol% of platelets is sufficient to reach 60–80% of the maximum measured reflectance. This trend can be empirically described using a simple analytical relation (Figure 4d–f; see Table S1 in Supporting information). To understand the effect of the volume fraction of platelets on the total reflectance, we performed analytical calculations on a model composite using the transfer matrix method.

2.4. Modelling of the Composite Optical Properties

To identify the main geometrical and material parameters that control the optical reflectance of the composites, we extended the optical model of single infinite platelets (Figure 3c) to systems containing up to thirty platelets embedded in an epoxy matrix (**Figure 5**a). In the composite model, the platelets and the epoxy phase were considered as flat micro-reflectors and the cavity medium, respectively. A unit cell was defined to consist of a platelet with an upper epoxy layer so that the reflectance of composites with a well-defined number of platelets (N) can be computed (Figure 5b).

Transfer-matrix calculations were performed on the model composites to evaluate the effect of the epoxy thickness (d_{ep}), platelet thickness (b), the thickness of the titania coating (δ), the number of platelets (N), as well as the platelet volume fraction (ϕ) on the optical reflectance of the composite. The calculated results were then compared to the experimental data to shed light on the parameters controlling the optical response of the composite.

The calculated reflectance spectra exhibit characteristic mode spectra of an FP resonator (Figure 5c,d,g), including the oscillations resulting from interference phenomena. While these oscillations are smeared out by scattering effects in the disordered composite, we display the raw calculated spectra for sake of clarity. In contrast to individual platelets, where the FSR and linewidth were dependent on the alumina thickness, here both depend on the epoxy thickness (Figure 5c). This is an important

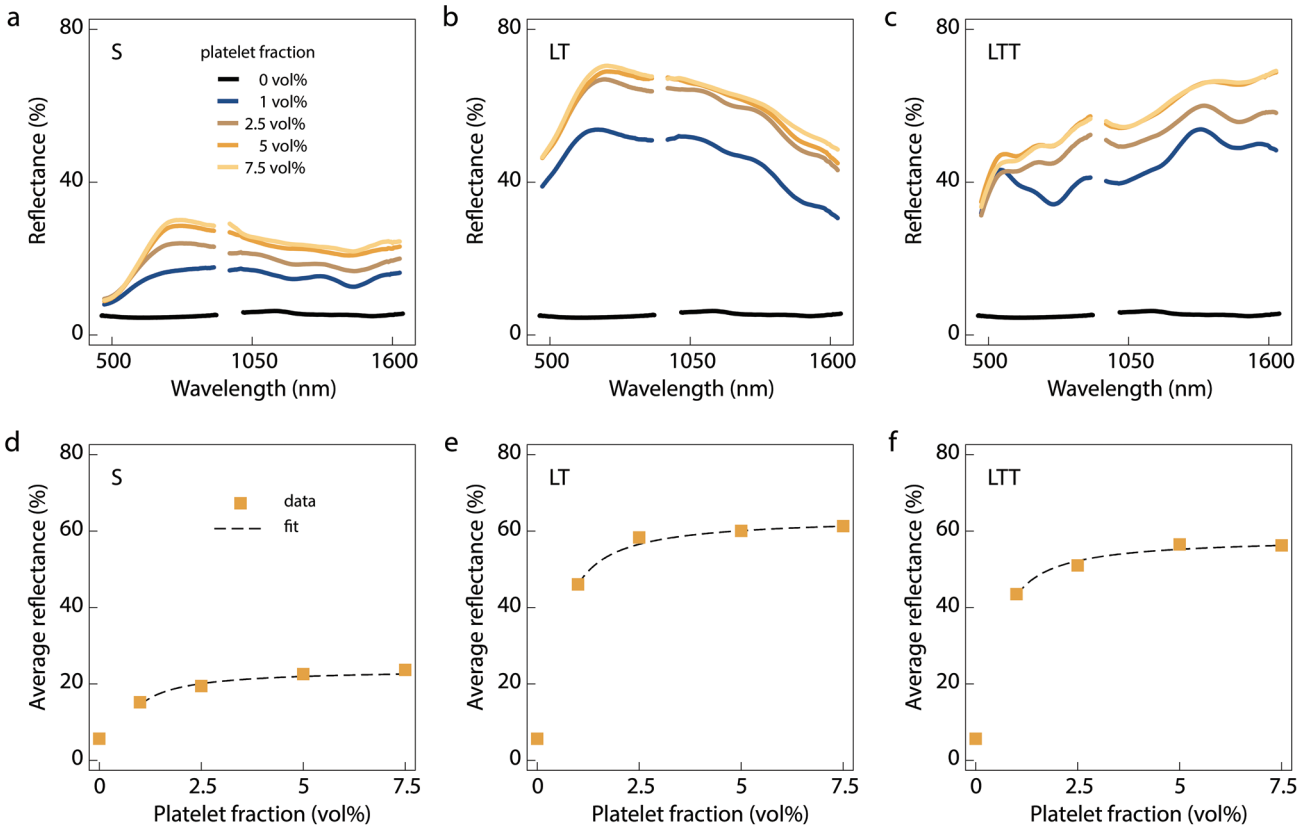

Figure 4. Experimentally measured diffuse reflectance of composites containing aligned microplatelets. Reflectance spectra for composites containing increasing volume fractions of a) S, b) LT, and c) LTT platelets. Reflectance data averaged over the wavelength range 450–900 nm and 1000–1630 nm as a function of the platelet volume fraction for d) S, e) LT, and f) LTT platelets.

result, as it indicates that the epoxy acts as a cavity medium and the microplatelets as semi-transparent flat reflectors in the FP resonator. The reflectance and the dispersion of these micro-reflectors can be engineered by changing the thickness of the platelets, which blue-shifts the reflectance spectra similarly to what was observed for individual platelets (Figure 3d). Coating the alumina platelets with a titania layer of increasing thickness (δ) changes the reflectance curves of the flat micro-reflectors in a similar way (Figure 5d).

The thickness of the titania layer (δ) also influences the spectral-averaged reflectance of platelet stacks. The reflectance of a stack of six platelets steadily increases with δ up to a titania layer thickness of ≈75 nm (Figure 5e). Above this thickness, the reflectance reaches a plateau that only depends on the volume fraction of platelets. The enhanced reflectance of composites with titania-coated platelets arises from the higher refractive index of this oxide compared to alumina, making these microplatelets more effective in reflecting the incoming light. In these calculations, each data point corresponds to the average of the reflectance calculated for platelets with alumina thickness in the range of 200–400 nm.

Since the commercial platelets exhibit a thickness distribution between 200–400 nm, composites containing such platelets should display a broad reflectance spectrum determined by multiple contributions of platelets of distinct, different thicknesses. Indeed, a comparative analysis of the reflectance data reveals a good agreement between the calculated spectra and the experimental results, when calculations from multiple LT platelets of different coating thicknesses are averaged (Figure 5f, see Materials and methods). The lower experimental reflectance observed at wavelengths below 700 nm is likely caused by the interaction of light with the SPIONs that are used to functionalize the platelets, as the extinction coefficient of suspensions of iron oxide nanoparticles has been shown to steadily increase when the wavelength is decreased from 800 to 450 nm.[35,36]

In terms of the number of platelets (unit cells), our calculations indicate that the reflectance of the model composites increases sharply by increasing the number of unit cells (N) up to ≈10 (Figure 5g,h). Beyond ≈10 platelets, the reflectance at a given wavelength was found to reach a plateau. This suggests that the multiple reflection events expected in thicker structures cause attenuation of the traveling light wave due to the lossy nature of the coated platelets and the epoxy matrix. As a result, only a limited number of platelets (N_{loss}) is able to act as micro-reflectors and contribute to the total reflectance of the composite.

2.5. Angular Distribution of Platelets in Composites

To gain insight into the origin of the incoherence effects that average out the optical response of the composite (Figure 5f),

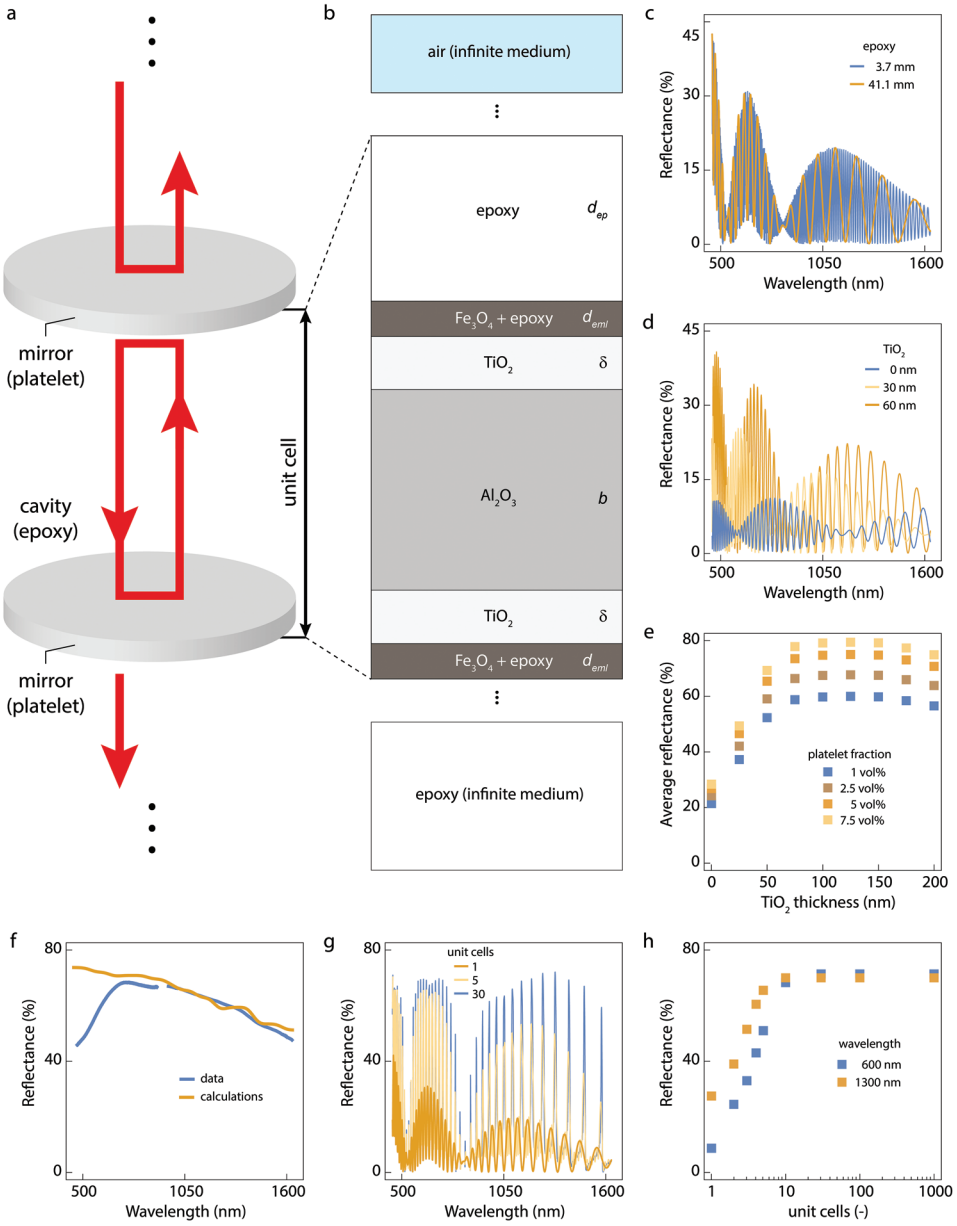

Figure 5. Analytical modeling of the optical reflectance of composites containing aligned microplatelets. a) Schematics of the platelets embedded in epoxy, acting as flat micro-reflectors and cavities in a Fabry–Pérot resonator, respectively. b) Schematics of the model composite analyzed with the transfer-matrix method. A unit cell is defined such that the model can compute the reflectance of stacked platelets. Influence c) of the epoxy thickness (d_{ep}) in 325-nm thick alumina platelets coated with a 45-nm thick titania layer and d) of the thickness of the titania coating (δ) in 325-nm thick alumina platelets on the reflectance spectra of composites containing 1 unit cell. e) Reflectance of composites as a function of the thickness of the titania coating averaged for platelets with alumina thickness in the range 200–400 nm. f) Comparison between the calculated and experimental reflectance spectra for composites with LT platelets of varying thicknesses. The effect of the number of platelets (unit cells) on g) the reflectance spectra and h) the average reflectance at two specific wavelengths of composites for platelets with a 45-nm thick titania coating.

we analyze the angular distribution and spacing of the microplatelets inside the polymer matrix.

The angular distribution of platelets in the composite is often directly related to the manufacturing process. In this work, the platelet angular distribution was quantified via image analysis of scanning electron micrographs of cross-sections of composites containing up to 7.5 vol% LT platelets (SEM, **Figure 6**a–c). Platelets are readily visible as white features embedded in a grey-colored epoxy background. The color contrast arises from the higher atomic number of the oxide platelets compared to the epoxy, which allows us to assess the angular distribution of the platelets by applying a Fourier transform to the images (insets of Figure 6a–c). The Fourier transforms of the SEM images clearly capture the alignment of the platelets parallel to

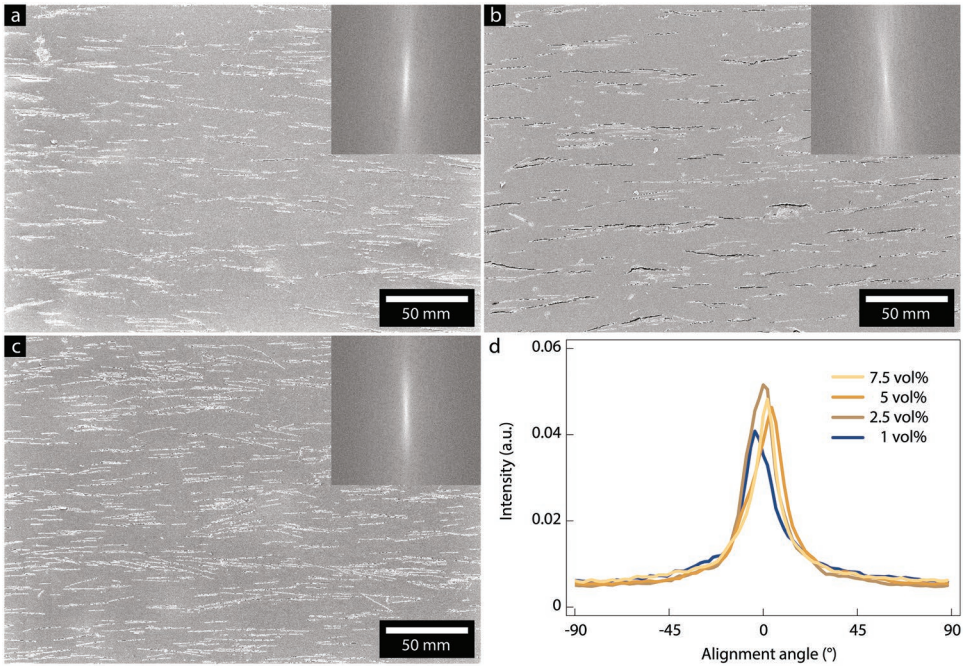

Figure 6. Angular distribution of microplatelets in composites. Electron microscopy images of the cross sections of composites containing a) 1, b) 5, and c) 7.5 vol% of magnetically aligned LT platelets in epoxy. The insets display the Fast Fourier Transform of the images. d) Platelet angular distributions of composites with increasing concentration of LT platelets.

the surface of the composite, as indicated by the vertical patterns formed in reciprocal space.

To quantify the average orientation θ and its standard deviation s of the platelets, we measured the local orientation of a large number of platelets observed in SEM cross-sections using an image analysis algorithm (see Experimental Section). The algorithm confirms the strong alignment of platelets parallel to the sample surface (Figure 6d), evidenced by the small variation of the average alignment θ between –2.1 and 2.2° relative to the surface normal (Table S2, Supporting Information). The standard deviation of the alignment s, a measure of the misalignment of the platelets, was found to be in the range of 7–10°. Interestingly, the orientation parameter does not show any clear correlation with the volume fraction of platelets, suggesting that the magnetic alignment approach is robust for the whole range of investigated concentrations.

The experimentally measured angular distribution of platelets can be used to estimate the number of platelets that are expected to contribute to the reflectance of the composite. The underlying assumption is that platelet misalignment is expected to reduce the directional reflectance of the composite by scattering the light wave away from its original direction, thus preventing reflection back to the viewer and creating a more diffusive, less glossy appearance.

To evaluate the effect of platelet misalignment on the reflectance of the composite, we analytically determine the critical number of platelets N^* at which a light ray is reflected before it fully deviates from its original direction. In this analysis, the platelet angular distribution in a composite is approximated by a normal distribution $\mathcal{N}(\theta,s)$ with mean θ and standard variation s. Even though the precise alignment angle θ_i of each platelet is unknown, its probability density function f_{θ_i} is described by the normal distribution of the composite $\mathcal{N}(\theta,s)$. After reflection by a series of platelets, the direction of a light ray will have a probability distribution function that depends on θ, s, and on the number of reflections. This probability distribution function of light direction can be calculated after each reflection and becomes wider as the number of reflection events increases (see Figure S4, Supporting information). More specifically, after N reflection events, this probability distribution function is $\mathcal{N}(\theta,2\sqrt{N}s)$. Considering that the direction of the light ray becomes random when its probability distribution function is predominantly flat in the range (–90°,90°), we can find the number of reflections N^* to reach this condition by setting the standard deviation to 90°. This means that only half of the light contributes to the reflectance of the composite after being reflected N^* times. Following this rationale, N^* can be expressed by:

$$N^* = \left(\frac{45^\circ}{s}\right)^2 \tag{1}$$

Taking the experimentally measured standard deviation s (Figure 6d), we apply our simple analytical model (Equation 1) to estimate the number of reflection events N^* that should contribute to the total reflectance of composites with one specific type of platelet (Table S2, Supporting Information). The analysis reveals that the level of alignment achieved by the manufacturing process allows for a maximal 23 to 38 LT platelets to contribute to the optical reflectance of the composite, depending on the platelet concentration.

By comparing the N^* values obtained from this analysis ($23 < N^* < 38$) with the N_{loss} value predicted by calculations ($N_{loss} = 10$), we conclude that the critical number of platelets needed to fully attenuate the traveling light is smaller than the number of aligned platelets that could potentially contribute to reflecting the incoming light. This indicates that the lossy character of the platelets and matrix materials plays a dominant role that limits the total reflectance of the composite. Further improvements in reflectance are therefore expected by reducing the losses in the platelets while keeping the strong orientation achieved through the magnetic alignment process. Lower losses might be achieved by selecting platelets with a lower imaginary part of the refractive index and/or by optimizing the SPION concentration to reduce light absorption without compromising platelet alignment.

3. Conclusions

The optical reflectance of composites containing in-plane oriented alumina platelets is strongly influenced by the material and geometrical properties of the embedded platelets. Analytical calculations based on the transfer-matrix method can be reliably used to interpret the experimental reflectance data of both individual platelets and platelet-containing macroscopic composites. A comparison between modeling and experiments reveals that the number of platelets that contribute to the composite reflectance is determined by the level of alignment resulting from the manufacturing process as well as by optical losses arising from multiple reflections inside the engineered platelets. On the one hand, in-plane alignment increases the number of platelets that contribute to the reflectance of the composite. On the other hand, lossy platelets reduce the composite reflectance by decreasing the intensity of the propagating light through absorption. For the manufacturing process investigated in this study, we found that the lossy character of the platelets limits the optical reflectance of the composites. The agreement between the analytical model and experiments indicates that the assumptions considered in the idealized composite are appropriate to describe the interactions of light with the spatially distributed platelets. Experiments and modeling reveal that a large refractive index mismatch between the platelets and the continuous matrix, platelet alignment, and a wide platelet thickness distribution are essential requirements to enhance the broadband reflectance of the composites. These findings should aid the design and selection of materials and manufacturing routes for the creation of synthetic composites with tunable optical reflectance. Because platelet alignment can also be achieved by simple shear, our composite model is relevant for a broad range of established or novel applications, including reflective coatings and paints for radiative cooling, structural color formation, and thermal management.

4. Experimental Section

The epoxy-platelets composites were fabricated with bare and titania-coated alumina platelets (RonaFlair and Xirallic lines, Merck KGaA), ferrofluid (EMG series, Ferrotec GmbH), and epoxy resin (Specifix-20 Kit, Struers GmbH). Table 1 shows the dimensions of the alumina platelets used and the approximated thicknesses of their titania coatings.

Bare and titania-coated alumina platelets were magnetically functionalized by the adsorption of superparamagnetic iron oxide nanoparticles (SPIONs) from EMG 705 and EMG 605 ferrofluids, respectively. Different fractions of the magnetized platelets (1, 2.5, 5, and 7.5 vol%) were added to epoxy resin and the formed suspensions were mixed and degassed in a planetary mixer (ARE-250, Thinky) for homogenization. These suspensions were poured into cylindrical silicone molds with an internal diameter of 25 mm for the alignment and curing steps. The filled molds were immediately placed in a custom-made alignment setup consisting of a shaker (Vortex-Genie 2, Scientific Industries Inc.) and a neodymium magnet (Death Magnet, Supermagnete) rotated at 3 Hz by an electric motor. The curing process lasted 12 h in total and was carried out at room temperature. In the first 5 min, the suspensions in the molds were exposed to both the mechanical vibrations of the shaker and the in-plane rotating magnetic field lines generated by the motor-driven magnet. The shaker was then turned off and the magnetic field was left on until the end of the curing step. Subsequently, the cured composites were released from the molds and longitudinally cut with a diamond saw (Accutom-100, Struers) at 7 mm from their upper surfaces. The cut surfaces were mirror-polished (LaboPol-25, Struers) with silicon carbide grinding papers and water-based diamond suspensions.

The spectral reflectance of the mirror-polished composite surfaces was measured with setups for specular and diffuse reflectometry. The specular reflectance (Figure 2d–f) was measured by illuminating the sample with collimated white light from a deuterium-halogen light source (DH-2000-BAL, Ocean Insight Inc.). The sample was mounted on a rotating stage and the angle between the incident light and the normal to the sample surface was fixed at 20°. The size of the illuminated spot was fixed by using a 3-mm aperture between the sample and the collimating lens at the surface of the optical fiber. A spectrometer (QE Pro High-Performance Spectrometer, Ocean Insight Inc.) mounted on a rotating arm was used to scan different angles ≈20° from the surface normal to measure the specular reflectance of the sample. The diffuse reflectance (Figures 5f and 4a–c) was measured using spectrometers (Flame-S and Flame-NIR, Ocean Insight Inc.) connected to an integrating sphere (ISP-50-8-R-GT, 50 mm, Ocean Insight Inc.). The samples were illuminated by a tungsten halogen source (HL-2000-HP-FHSA, Ocean Insight Inc.).

The spectral reflectance measurements of single platelets (Figure 3a,b) were performed using a xenon light source (Thorlabs SLS401, Thorlabs GmbH) and a light microscope (ZEISS Axio Scope.A1, Zeiss AG) equipped with an objective (Zeiss Epiplan Apochromat 20×, NA 0.6, Zeiss AG). The light reflected from the sample was collected with an optical fiber (QP50-2-UV-BX, 230 µm core, Ocean Insight Inc.), resulting in a measurement spot diameter of ≈20 µm. The spectra were recorded by a diode spectrometer (QE 65 Pro, Ocean Insight Inc.).

A broadband mirror and a scatterer were used as a reference for all specular and diffuse reflectance measurements, respectively. Spectra were also acquired with the shutter closed to block the incident light (dark noise). The reflectance was calculated as the ratio between the reflected intensity minus dark noise and the reference spectrum minus dark noise.

The composite cross-sections were imaged with a scanning electron microscope (LEO 1530 Gemini, Zeiss) (Figure 6a–c) and their upper surfaces with a light microscope (Polyvar Met, Reichert Inc.) (Figure 2g). Platelet orientation distributions and their alignment parameters were calculated with the plug-in "Directionality" of the free software Fiji (Figure 6d; Table S2, Supporting Information).[37]

The spectral reflectance of single platelets and of composites containing multiple platelets was computed with the transfer-matrix method[20] and implemented in the software Mathematica (Wolfram Research, Inc., Mathematica, Version 13.0.0, Champaign, IL, 2021). In the calculations, the reflection and transmission coefficients for *s* and

p polarized light traveling from medium *i* to medium *j* are given by the Fresnel equations:

$$r_s(\lambda,\theta)=\frac{n_i(\lambda)\cos\left(\sin^{-1}\left(\frac{n_0(\lambda)}{n_i(\lambda)}\sin\theta\right)\right)-n_j(\lambda)\cos\left(\sin^{-1}\left(\frac{n_0(\lambda)}{n_j(\lambda)}\sin\theta\right)\right)}{n_i(\lambda)\cos\left(\sin^{-1}\left(\frac{n_0(\lambda)}{n_i(\lambda)}\sin\theta\right)\right)+n_j(\lambda)\cos\left(\sin^{-1}\left(\frac{n_0(\lambda)}{n_j(\lambda)}\sin\theta\right)\right)}$$

$$r_p(\lambda,\theta)=\frac{n_j(\lambda)\cos\left(\sin^{-1}\left(\frac{n_0(\lambda)}{n_j(\lambda)}\sin\theta\right)\right)-n_i(\lambda)\cos\left(\sin^{-1}\left(\frac{n_0(\lambda)}{n_i(\lambda)}\sin\theta\right)\right)}{n_i(\lambda)\cos\left(\sin^{-1}\left(\frac{n_0(\lambda)}{n_j(\lambda)}\sin\theta\right)\right)+n_j(\lambda)\cos\left(\sin^{-1}\left(\frac{n_0(\lambda)}{n_i(\lambda)}\sin\theta\right)\right)}$$

$$t_s(\lambda,\theta)=\frac{2n_i(\lambda)\cos\left(\sin^{-1}\left(\frac{n_0(\lambda)}{n_i(\lambda)}\sin\theta\right)\right)}{n_i(\lambda)\cos\left(\sin^{-1}\left(\frac{n_0(\lambda)}{n_i(\lambda)}\sin\theta\right)\right)+n_j(\lambda)\cos\left(\sin^{-1}\left(\frac{n_0(\lambda)}{n_j(\lambda)}\sin\theta\right)\right)}$$

$$t_p(\lambda,\theta)=\frac{2n_i(\lambda)\cos\left(\sin^{-1}\left(\frac{n_0(\lambda)}{n_i(\lambda)}\sin\theta\right)\right)}{n_i(\lambda)\cos\left(\sin^{-1}\left(\frac{n_0(\lambda)}{n_j(\lambda)}\sin\theta\right)\right)+n_j(\lambda)\cos\left(\sin^{-1}\left(\frac{n_0(\lambda)}{n_i(\lambda)}\sin\theta\right)\right)} \quad (2)$$

where reflection and transmission coefficients are denoted by *r* and *t*, respectively, and their subindices correspond to the *s* or *p* light polarization. The coefficients depend on the wavelength λ and on the angle of the incident light θ relative to the normal of the platelet or specimen surface. The complex refractive indices of the embedding medium and of the media *i* and *j* are $n_0(\lambda)$, $n_i(\lambda)$ and $n_j(\lambda)$, respectively. Note that θ_i and θ_j, the angles of light traveling in the media *i* and *j*, are given as a function of the refractive indices and θ using Snell's law, $n_0 \sin\theta = n_i \sin\theta_i = n_j \sin\theta_j$. Additionally, the phase thickness imposed by propagating through medium *i* is given by $\beta(\lambda, \theta, h_i)$:

$$\beta(\lambda,\theta,h_i)=\frac{2\pi\, n_i(\lambda)\, h_i}{\lambda}\cos\left(\sin^{-1}\left(\frac{n_0(\lambda)}{n_i(\lambda)}\sin\theta\right)\right) \quad (3)$$

where h_i is the thickness of the layer composed of medium *i*. The matrices used in the transfer-matrix method are defined from the coefficients and the phase thickness in Equations 2 and 3.[20] These matrices are denoted by M_s, M_p and *P* and account for light crossing the interface between media *i* and *j* in the *s* and *p* polarizations and for light propagating through a medium *i*, respectively:

$$M_s(\lambda,\theta)=\frac{1}{t_s(\lambda,\theta)}\begin{bmatrix}1 & r_s(\lambda,\theta)\\ r_s(\lambda,\theta) & 1\end{bmatrix}$$

$$M_p(\lambda,\theta)=\frac{1}{t_p(\lambda,\theta)}\begin{bmatrix}1 & r_p(\lambda,\theta)\\ r_p(\lambda,\theta) & 1\end{bmatrix} \quad (4)$$

$$P(\lambda,\theta,h_i)=\begin{bmatrix}e^{-i\beta(\lambda,\theta,h_i)} & 0\\ 0 & e^{i\beta(\lambda,\theta,h_i)}\end{bmatrix}$$

The matrices in Equation 4 can be defined for light crossing or propagating through different media. To account for the path of the incident polarized light wave through all the layers of the studied system, the matrices can be multiplied in the order of appearance of the layers. This product yields the transfer matrices T_s and T_p for the *s* and *p* polarized light, respectively, which were different for a system consisting of a single platelet (Figure 3c) or multiple platelets (Figure 5a,b). In both systems, the reflectance *R* was defined from the transfer matrices T_s and T_p:

$$R(\lambda,\theta)=\frac{1}{2}\left|\frac{T_s[2,1]}{T_s[1,1]}\right|^2+\frac{1}{2}\left|\frac{T_p[2,1]}{T_p[1,1]}\right|^2 \quad (5)$$

For single platelets, a multilayer structure with the geometrical and optical parameters of each platelet was used for the calculations (Figure 3c). A glass slide with thickness of 1 mm was considered in the calculations so that they could be directly compared to the reflectance spectra of single platelets (Figure 3a,b; Figure S1a, Supporting Information) acquired experimentally. The transfer matrices corresponding to this structure were defined by:

$$T_s = T_p = M_{1,5}\, P_5 M_{5,2} P_2 M_{2,3} P_3 M_{3,2} P_2 M_{2,5} P_5 M_{5,1} P_1 M_{1,4} P_4 M_{4,1} \quad (6)$$

where the subindices 1, 2, 3, 4, and 5 correspond, respectively, to the media air, titania, alumina, glass, and the effective layer formed by iron oxide and air. The matrices T_s and T_p were equal because the refractive indices used for the different components did not change with light polarization. For simplicity, the dependency on λ and θ was omitted in Equation 6.

Analogously, multilayer structures were used for calculating the reflectance of composites. The structure corresponding to a single platelet and its adjacent epoxy layer was defined as a unit cell to allow for computing the contribution of stacks of multiple platelets (Figure 5a,b). The reflectance of each stack was calculated with the following transfer matrices:

$$T_s = T_p = M_{1,4}\left(P_4 M_{4,5} P_5 M_{5,2} P_2 M_{2,3} P_3 M_{3,2} P_2 M_{2,5} P_5 M_{5,4}\right)^N \quad (7)$$

where the subindices 1, 2, 3, 4, and 5 correspond, respectively, to the media air, titania, alumina, epoxy, and the effective layer formed by iron oxide and air. The unit cell is given between parentheses and its contribution to the reflectance is determined by the number of platelets in the stack, *N*. Similarly to Equation 6, the dependency on λ and θ was omitted and the refractive indices do not change with light polarization, resulting in equal transfer matrices ($T_s = T_p$). Because platelets of the same type had variations in their geometry (Table 1), the reflectance of composites considered different stacks of platelets with constant thicknesses within each stack. To calculate the reflectance of a composite containing 5 vol% of LT platelets, four stacks of thirty platelets with fixed thicknesses for the titania ($\delta = 45$ nm), effective medium ($d_{eml} = 12$ *nm*) and epoxy ($d_{ep} = 4.5$ µm) layers were considered. The epoxy layer was calculated using the dimensions of LT platelets and $\varphi = 5$ vol% (see Supporting information). The four stacks had different thicknesses of the alumina layer (*b*): 175, 250, 325 and 400 nm. First, the reflectance of each stack was calculated. Next, the curves corresponding to their upper envelopes were taken to smear out the multiple high-order oscillations (Figure 5c,d; Figure S4a,b, Supporting Information). Finally, these curves were averaged to generate the calculated reflectance of a composite of LT platelets (Figure 5f).

Supporting Information

Supporting Information is available from the Wiley Online Library or from the author.

Acknowledgements

The authors thank the Swiss National Science Foundation for the financial support through project number 200021_160184 and through

the National Center of Competence in Research (NCCR) Bio-Inspired Materials (Grant No. 51NF40-182881). Prof. Dr. Eric Dufresne and Dr. Robert Style (ETH Zürich) were greatly acknowledged for their fruitful discussions.

Conflict of Interest

The authors declare no conflict of interest.

Data Availability Statement

The data that support the findings of this study are available from the corresponding author upon reasonable request.

Keywords

alumina, epoxy, manufacturing, reflective materials, titania

Received: August 25, 2022
Revised: November 14, 2022
Published online:

[1] G. Pfaff, P. Reynders, *Chem. Rev.* **1999**, *99*, 1963.
[2] F. Schenk, B. D. Wilts, D. G. Stavenga, *Bioinspiration Biomimetics* **2013**, *8*, 045002.
[3] E. Rephaeli, A. Raman, S. Fan, *Nano Lett.* **2013**, *13*, 1457.
[4] A. P. Raman, M. A. Anoma, L. Zhu, E. Rephaeli, S. Fan, *Nature* **2014**, *515*, 540.
[5] R. F. Brady, L. V. Wake, *Prog. Org. Coat.* **1992**, *20*, 1.
[6] E. Poloni, A. Rafsanjani, V. Place, D. Ferretti, A. R. Studart, *Adv. Mater.* **2021**, *34*, 2104874.
[7] B. A. Slovick, J. M. Baker, Z. Flom, S. Krishnamurthy, *Appl. Phys. Lett.* **2015**, *107*, 141903.
[8] N. P. Padture, M. Gell, E. H. Jordan, *Science* **2002**, *296*, 280.
[9] J. D. Joannopoulos, S. G. Johnson, J. N. Winn, R. D. Meade, *Photonic Crystals: Molding the Flow of Light*, 2nd ed., Princeton University Press, Princeton, NJ **2011**.
[10] S. Kinoshita, *Structural Colors in the Realm of Nature*, World Scientific, Singapore **2008**.
[11] M. Srinivasarao, *Chem. Rev.* **1999**, *99*, 1935.
[12] L. P. Biró, J. P. Vigneron, *Laser Photonics Rev.* **2011**, *5*, 27.
[13] D. Gur, B. A. Palmer, B. Leshem, D. Oron, P. Fratzl, S. Weiner, L. Addadi, *Angew. Chem. Int. Ed.* **2015**, *54*, 12426.
[14] L. M. Mäthger, G. R. R. Bell, A. M. Kuzirian, J. J. Allen, R. T. Hanlon, *J. Exp. Biol.* **2012**, *215*, 3752.
[15] D. Gur, E. J. Bain, K. R. Johnson, A. J. Aman, H. A. Pasolli, J. D. Flynn, M. C. Allen, D. D. Deheyn, J. C. Lee, J. Lippincott-Schwartz, D. M. Parichy, *Nat. Commun.* **2020**, *11*, 6391.
[16] H. G. Frohnhöfer, J. Krauss, H.-M. Maischein, C. Nüsslein-Volhard, *Development* **2013**, *140*, 2997.
[17] Z. Luo, B. A. Evans, C.-H. Chang, *ACS Nano* **2019**, *13*, 4657.
[18] S. Chen, L. Yuan, X. Weng, L. Deng, *Infrared Phys. Technol.* **2014**, *67*, 377.
[19] P. S. Mudgett, L. W. Richards, *Appl. Opt.* **1971**, *10*, 1485.
[20] C. C. Katsidis, D. I. Siapkas, *Appl. Opt.* **2002**, *41*, 3978.
[21] P. Yeh, *Optical Waves in Layered Media*, Wiley, Hoboken, NJ **2005**.
[22] P. Markos, C. M. Soukoulis, *Wave Propagation: From Electrons to Photonic Crystals and Left-Handed Materials*, Princeton University Press, Princeton, NJ **2008**, pp. 181–198.
[23] J. L. Ocana-Pujol, L. Forster, R. Spolenak, H. Galinski, *Adv. Opt. Mater.* **2022**, https://doi.org/10.1002/adom.202201749.
[24] G. M. Paternò, C. Iseppon, A. D'Altri, C. Fasanotti, G. Merati, M. Randi, A. Desii, E. A. A. Pogna, D. Viola, G. Cerullo, F. Scotognella, I. Kriegel, *Sci. Rep.* **2018**, *8*, 3517.
[25] K. Sasaki, K. Hitachi, *Commun. Physics* **2020**, *3*, 90.
[26] R. M. Erb, R. Libanori, N. Rothfuchs, A. R. Studart, *Science* **2012**, *335*, 199.
[27] H. Le Ferrand, F. Bouville, T. P. Niebel, A. R. Studart, *Nat. Mater.* **2015**, *14*, 1172.
[28] H. Le Ferrand, F. Bouville, A. R. Studart, *Soft Matter* **2019**, *15*, 3886.
[29] G. Pfaff, *Chemie&more* **2013**, *6*, 33.
[30] M. Born, L. N. L. M. Born, E. Wolf, M. A. X. A. BORN, A. B. Bhatia, P. C. Clemmow, D. Gabor, A. R. Stokes, A. M. Taylor, P. A. Wayman, *Principles of Optics: Electromagnetic Theory of Propagation, Interference, and Diffraction of Light*, Cambridge University Press, Cambridge, England **1999**.
[31] J. C. M. Garnett, *Philos. Trans. Royal Soc. A, Containing Papers of a Mathematical or Physical Character* **1904**, *203*, 385.
[32] M. R. Querry, *Optical constants, Contractor Report (Sep. 1982–May 1984)*, Missouri University, Kansas **1985**.
[33] S. Sarkar, V. Gupta, M. Kumar, J. Schubert, P. T. Probst, J. Joseph, T. A. F. König, *ACS Appl. Mater. Interfaces* **2019**, *11*, 13752.
[34] R. M. Erb, J. Segmehl, M. Charilaou, J. F. Loffler, A. R. Studart, *Soft Matter* **2012**, *8*, 7604.
[35] C. Boxall, G. Kelsall, Z. Zhang, *J. Chem. Soc., Faraday Trans.* **1996**, *92*, 791.
[36] E. Y. Levitin, N. G. Kokodiy, V. A. Timanjuk, I. O. Vedernikova, T. M. Chan, *Inorg. Mater.* **2014**, *50*, 817.
[37] J. Schindelin, I. Arganda-Carreras, E. Frise, V. Kaynig, M. Longair, T. Pietzsch, S. Preibisch, C. Rueden, S. Saalfeld, B. Schmid, J.-Y. Tinevez, D. J. White, V. Hartenstein, K. Eliceiri, P. Tomancak, A. Cardona, *Nat. Methods* **2012**, *9*, 676.